CLIMATOLOGY

Making climate projections conditional on historical observations

Aurélien Ribes[1]*, Saïd Qasmi[1], Nathan P. Gillett[2]

Many studies have sought to constrain climate projections based on recent observations. Until recently, these constraints had limited impact, and projected warming ranges were driven primarily by model outputs. Here, we use the newest climate model ensemble, improved observations, and a new statistical method to narrow uncertainty on estimates of past and future human-induced warming. Cross-validation suggests that our method produces robust results and is not overconfident. We derive consistent observationally constrained estimates of attributable warming to date and warming rate, the response to a range of future scenarios, and metrics of climate sensitivity. We find that historical observations narrow uncertainty on projected future warming by about 50%. Our results suggest that using an unconstrained multimodel ensemble is no longer the best choice for global mean temperature projections and that the lower end of previous estimates of 21st century warming can now be excluded.

INTRODUCTION

In 2018, the special report of the Intergovernmental Panel on Climate Change (IPCC) on global warming of 1.5°C (1) stated that "human activities [...] have caused approximately 1.0°C of global warming above pre-industrial levels." Climate change is now well under way. As the global warming signal increases, observations provide increasingly accurate information about how the climate system responds to an increase in atmospheric greenhouse gases (GHGs) concentrations and other human factors. Consequently, there is growing interest in monitoring ongoing climate change and providing near-term and long-term projections that are consistent with the latest observations.

First attempts to constrain projections from historical observations were based on detection and attribution (D&A) techniques (2–5), i.e., estimates of how much past warming is attributable to human influence on climate. Although recent such analyses reported a downward revision of the upper bound of projected warming (6, 7), these studies primarily find a modest narrowing of uncertainties. As a result, the expected 21st century warming in response to various scenarios was calculated directly from model outputs in the IPCC Fifth Assessment Report (AR5) (8), i.e., without any observational constraint. Other studies tried to constrain metrics of climate sensitivity, such as the transient climate response (TCR; i.e., the global mean warming at CO_2 concentration doubling, in response to a yearly 1% increase in CO_2 concentration) or the equilibrium climate sensitivity (ECS; i.e., the global mean warming at equilibrium after a doubling of CO_2 concentration) (9, 10), using energy balance models (11), or directly from Earth's energy budget (12). Although not all results agree (9), most of these studies also find a limited historical constraint and/or tend to modestly lower the range of values derived from climate models.

In an apparent contrast with the downward revision of the upper bound of the projected warming, the latest generation of climate models, from the Coupled Model Intercomparison Project Phase 6 (CMIP6) (13), exhibits higher sensitivity to CO_2 increase than the previous generation (14) (about 10% higher using the set of models considered in this study). As a result, the question of consistency between model projections and historical observations becomes even more critical for this new generation of models (15). Do the levels of warming previously estimated in response to a range of emission scenarios need to be revised upward? Or do historical observations rule out some of these simulations?

In this study, we reassess human-induced warming ranges that are consistent with historical observations in the past, in the near term and in the long term, and in light of three new factors: newly available climate models, improved observations, and a new statistical method.

Observations of near-surface atmospheric temperature (SAT) have been subject to major improvements recently. Commonly used datasets of observed temperature were based on spatially incomplete observations (16) and sea surface temperature (SST) instead of SAT over oceans (17). Together, these two effects have been shown to artificially reduce estimates of past warming by about 15%, with implications, e.g., in terms of remaining carbon budget (18). Accounting for these recent findings and improved observed data is critical to constrain future warming.

The statistical method is another key source of improvement over previous work. Most previous studies rely on linear regression techniques (2–7, 10) and do not consider model uncertainty in the spatial or temporal pattern (19, 20). Other constraints based on historical warming often focus on the trend over a specific subperiod (15), potentially neglecting useful information. A third approach relies on simple climate models in which parameter uncertainty can be explored comprehensively and then subselecting those trajectories that are consistent with historical observations (21, 22). Here, we use climate models of full complexity to provide a prior on the real-world forced response and then derive the posterior of this response, given the historical observations. This new statistical approach overcomes previous limitations: Model uncertainty is fully taken into account, and the entire observational record is used to constrain past and future responses to various external forcings in a consistent way.

Using these three components enables us to narrow uncertainties in climate change projections and suggests that the lower end of the IPCC AR5–projected warming ranges can now be excluded. Given

[1]CNRM, Université de Toulouse, Météo-France, CNRS, Toulouse, France. [2]CCCMA, Environment and Climate Change Canada, Victoria, BC, Canada.
*Corresponding author. Email: aurelien.ribes@meteo.fr

the high costs and damages associated with climate change impacts, mitigation, and adaptation, providing more accurate climate change projections, as is performed in this study, may offer substantial benefits to society.

RESULTS

Attributing recent warming

We first estimate the externally forced [i.e., all (ALL) forcings] warming to date. While this has often been performed using linear trends (7, 23), our technique can deal with a more complex temporal shape (determined by complex climate models) and account for some uncertainty on that shape. We find that the total forced warming is 1.09°C ± 0.14°C (all confidence ranges in this study are 5 to 95%), on average, over the 2010–2019 decade relative to the 1850–1900 preindustrial baseline (Fig. 1A) (24). This value is very close to the observed warming in GSAT (global and annual average of SAT) of 1.07 ° ± 0.07°C (considering observational uncertainty only) but exhibits larger uncertainty. If the calculation is performed for the year 2020 specifically (still relative to the 1850–1900 average), then the estimated total forced warming increases to 1.22 ° ± 0.16°C . These values are higher than previous estimates, which do not account for the effects of spatial coverage and/or SST blending (1, 25).

We then use the technique to narrow uncertainty on the warming attributable to various external forcings (Fig. 1A). Focusing on 2010–2019 again, we find that a very small fraction of the total forced warming, 0.06 ° ± 0.02°C, is attributed to natural (NAT) forcings—partly explained by reduced volcanic activity over the past decade, while the 1850–1900 base period was affected by the Krakatoa eruption. The warming induced by anthropogenic (ANT) forcings is close to the total forced response: 1.03 ° ± 0.15°C. The warming induced by GHGs only is estimated to be 1.42 ° ± 0.31°C and is partly offset by a cooling induced by other anthropogenic (OA) forcings (aerosols, ozone, and land use changes) of −0.39 ° ± 0.27°C. The observational constraint is particularly pronounced for the ALL and ANT components (uncertainty reduced by ~70% compared to the unconstrained ranges) and more modest for GHGs and OA (50 and 30% reduction, respectively). These results are consistent with previous assessment (23), although the quantification of temperature changes with respect to the preindustrial baseline is novel. Last, if compared to unconstrained ranges, then the constrained ranges essentially reject the highest responses to both GHGs and OA, and the smallest responses to GHGs are also ruled out.

A similar analysis can be applied to the 2010–2019 warming rate (Fig. 1B). The observed warming trend of 0.32 ° ± 0.01°C per decade (considering observational uncertainty only) is found to lie slightly above the upper end of the forced response (0.25 ° ± 0.05°C per decade). This suggests that internal variability has enhanced the warming trend over the past decade—consistent with the end of the global warming slowdown and a marked El Niño event in 2016. The current ANT-induced warming rate is estimated to be 0.22 ° ± 0.05°C per decade, which is slightly higher, and has narrower uncertainties than previous estimates (1, 25). Note that these numbers are derived using the Shared Socioeconomic Pathway (SSP) 2-4.5 scenario to extend historical simulations after 2014 and that even higher values are found if the SSP5-8.5 scenario is considered (fig. S5). We find a substantial NAT-induced warming trend over the past decade of 0.03 ° ± 0.01°C per decade, driven by both solar and volcanic activities. The GHG-induced warming rate, 0.23 ° ± 0.06°C per decade, is very
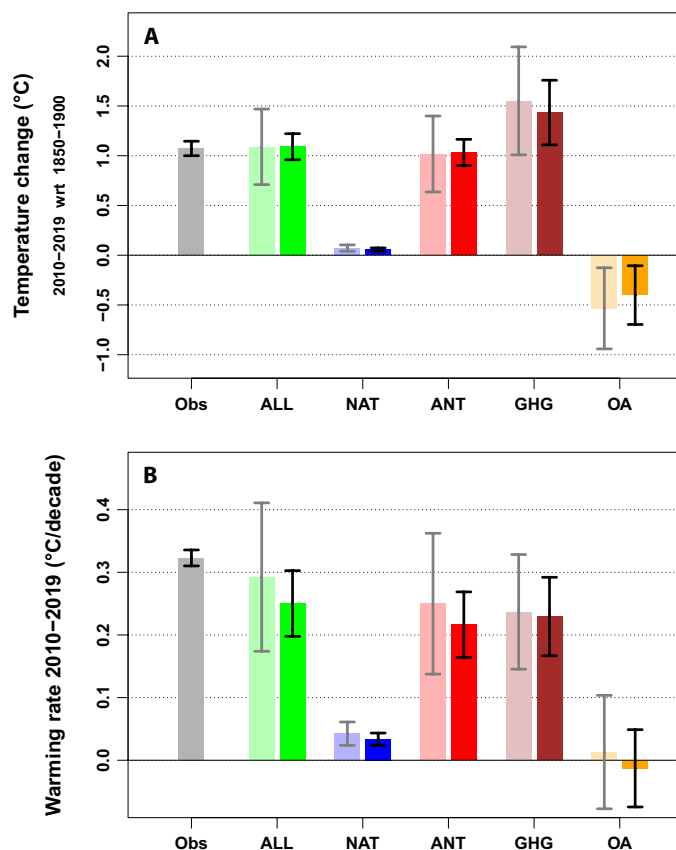

Fig. 1. Attribution results. (**A**) Changes induced by various subsets of external forcings over the historical period [2010–2019 with respect to (wrt) 1850–1900]. Observed (Obs) changes (gray, left) are deduced from Cowtan and Way (16) observations; uncertainty only includes observational uncertainty (i.e., measurement and processing; internal variability is ignored). For all other contributions, the left handside bar and gray confidence interval describe the CMIP6 model range, assuming a Gaussian distribution. The right handside bar and black confidence interval correspond to results constrained by observations. All ranges shown are 5 to 95% confidence ranges. The SSP2-4.5 scenario is used to extend historical simulations after 2014. (**B**) Same analysis for the 2010–2019 warming rate, computed as a linear trend over that period and expressed in degrees Celsius by decade.

close to model estimates. The sign of the OA contribution over the past decade is very uncertain, but the highest simulated rates of OA-induced warming are found to be inconsistent with the observational record. This analysis suggests that the partial offsetting of GHG-induced warming by the OA forcing since the preindustrial period was no longer active over the past decade, consistent with stabilized aerosol emissions over that period (11, 15).

Constraining projections

We now examine the implications of the observational constraint on the responses to specific scenarios such as the SSPs (26). In this respect, our procedure has some advantages compared to other observational constraint methods. Using the entire observed time series avoids ignoring useful information and facilitates annual updates. This also helps distinguish the responses to GHGs from OA factors, thanks to the different emission time series for these two subsets of forcings. In addition, the entire time series of constrained projections is derived in a consistent way, which is particularly attractive

for near-term projections (*23*). Last, our method enables us to provide confidence ranges specifically for the forced response, while many other studies also include internal variability.

We find that historical observations effectively constrain 21st century projections (Fig. 2). For all three scenarios considered, our observational constraint narrows the uncertainties (confidence interval widths) by a factor of about 2 at the end of the 21st century and by a factor of 3 in the short term (i.e., before 2040, consistent with the results for the externally forced warming to date). Such a large reduction in uncertainty is quite notable and is larger than that previously reported (*15*). Part of the discrepancy with other studies is related to the fact that our confidence ranges are representative of the forced response only, i.e., internal variability is filtered out, both before and after applying the observational constraint. But still, this finding raises questions about the robustness of our method, and whether it appropriately accounts for all sources of uncertainties (i.e., potential overconfidence).

To assess the robustness and predictive skill of our technique for the late 21st century warming, we perform a perfect model evaluation (*10*, *27*). We alternatively withhold one 1850–2100 transient run, treat its historical component (extended to 1850–2019) as pseudo-observations, and apply the method to predict the 2081–2100 SSP5-8.5 warming, using all other models to construct the prior—following a cross-validation procedure (more details are given in the Supplementary Materials). We use the coverage probability of our technique, i.e., the proportion of the time that the confidence interval contains the true value of interest, as a key criterion to evaluate its robustness. Results suggest that our statistical method is able to strongly decrease the uncertainty on future warming while preserving the desired confidence level (Fig. 3). We estimate a coverage probability of 86% giving equal weight to each single run (while 90% is expected), but this number is heavily influenced by the large CanESM5 (Canadian Earth System Model version 5) ensemble—a model that exhibits very high warming and is therefore more difficult to predict. Giving equal weight to each CMIP6 model (i.e., accounting for the unbalanced sizes of single-model ensembles), the estimate of coverage goes up to 91%, i.e., very close to the desired level. Evaluation of

our method using probabilistic scores provides consistent results (fig. S6). Furthermore, the method is able to correctly predict values that lie near the boundary or even outside the assumed 5 to 95% prior uncertainty range [see, e.g., GFDL (Geophysical Fluid Dynamics Laboratory)–ESM4 and CanESM5 models in Fig. 3]. Overall, these results demonstrate that our method is not overconfident and that the constrained uncertainty ranges are reliable. Nevertheless, this figure also suggests that some model responses might be harder to predict than others, i.e., the coverage probability for individual models can deviate from the desired 90%—although the coverage probability is correct if averaged over all CMIP6 models.

Beyond the overall level of reduction in uncertainties, the analysis of constrained ranges provides further insight (Figs. 2 and 4). In response to a moderately low emission scenario (SSP2-4.5), the constrained warming in 2100 is estimated to be 3 ° ± 0.7°C with respect to 1850–1900 (as compared to 3.2 ° ± 1.2°C for the unconstrained set of models). This range rises to 4.9 ° ± 1.1°C (and 5.4 ° ± 1.9°C for the unconstrained) in response to a high-emission scenario (SSP5-8.5). Human-induced warming is projected to exceed 1.5°C between 2027 and 2047 (best estimate, 2034), under SSP2-4.5. This range is consistent with extrapolating the estimates of ANT warming to date and ANT warming rate reported above.

Consistent with previous studies (*6*, *12*, *15*), we find that the upper end of model projected warming is not consistent with historical observations. More generally, the observational constraint revises unconstrained model projections downward, as central estimates are also lower after the constraint than before. However, unlike previous studies, we find that both sides of the uncertainty ranges are affected by the observational constraint, suggesting that both the highest and the lowest sensitivities inferred from the CMIP6 ensemble are inconsistent with observations. This finding is consistent with our results for the past GHG-induced warming. Then, if compared to the projected warming ranges from the IPCC AR5 (Fig. 4), then our late 21st century constrained ranges based on CMIP6 lie toward the upper end of previous estimates: Upper bounds are essentially unchanged, while lower bounds are revised upward. So, overall, our observational constraints revises the warming simulated by climate
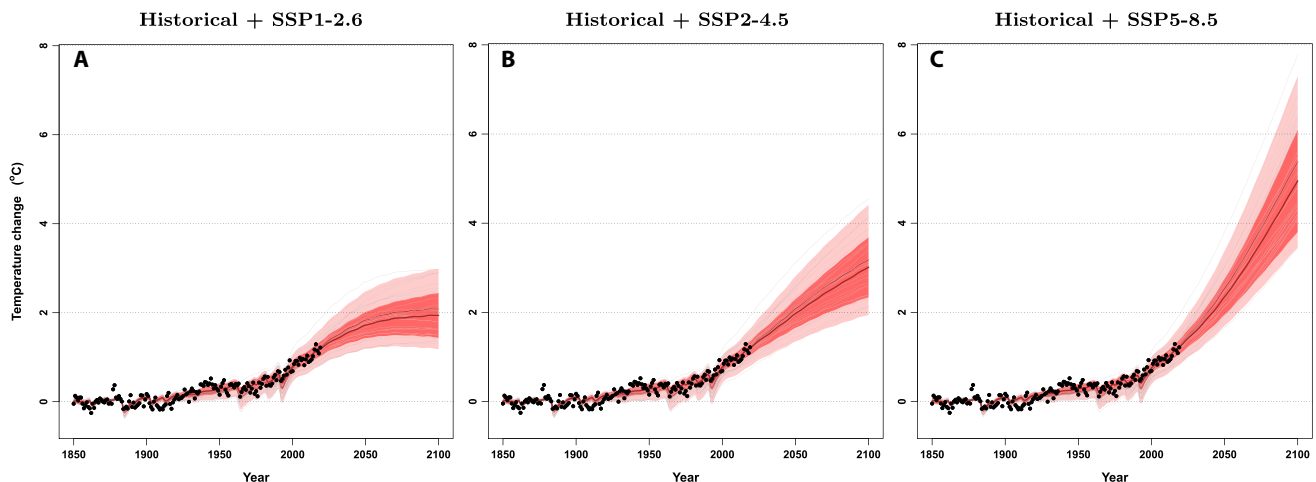

Fig. 2. Historical constraint on SSP projections. (A to **C)** The observational constraint is applied to concatenated historical and SSP scenarios simulations (SSP1-2.6, SSP2-4.5, or SSP5-8.5). Annually observed values of GSAT (black points) are compared to the unconstrained (pink) and constrained (red) 5 to 95% confidence ranges of forced response as estimated from 22 CMIP6 models. The time series of the forced responses of individual CMIP6 models are also shown (thin gray lines). All temperatures are anomalies with respect to the period 1850–1900.
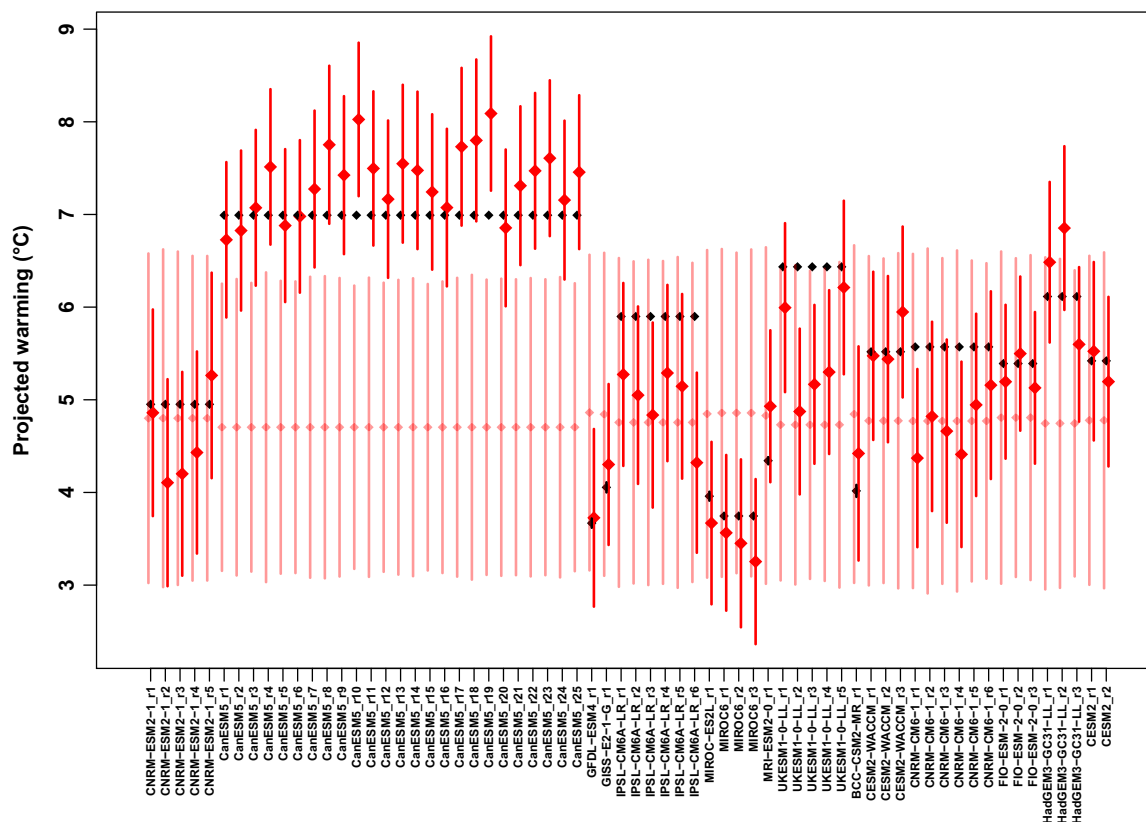
Fig. 3. Perfect model evaluation of the method. We consider 66 concatenated simulations of historical + SSP5-8.5 scenarios and use each of these to provide pseudo-observations over the historical period (1850–2019). The observational constraint is then applied to infer the 2081–2100 warming under this scenario. The effective warming, as estimated from the model ensemble mean after applying temporal smoothing, is shown in black (with 5 to 95% uncertainty). The unconstrained distribution is derived from all CMIP6 models, but the one used in pseudo-observations is shown in pink. The constrained distribution obtained after taking pseudo-observations into account is shown in red. Estimated that way, the coverage probability of our method (i.e., constrained ranges) is 86%, as opposed to 58% for the unconstrained ranges. However, both are strongly influenced by the large CanESM5 ensemble. Estimated coverage probabilities after giving equal weight to all models are 91 and 89%, respectively, for the constrained and unconstrained ranges.

models downward, while our observationally constrained projected warming ranges based on CMIP6 exclude the lower end of the AR5-assessed ranges.

Implications for climate sensitivity
Last, our methodology can be extended to constrain metrics of climate sensitivity such as the TCR and the ECS. Using CMIP6 models, we find a constrained TCR range of 1.84 ° ± 0.51°C, as compared to 1.98 ° ± 0.74°C without the constraint. Consistent with projections, the constrained range primarily revises the unconstrained CMIP6 range downward but excludes the lower end of the IPCC AR5–assessed likely range. The lower bound of our constrained range (i.e., 1.33°C) is consistent with some recent studies (21) but is quite high if compared to others (11, 15). One simple argument supporting our finding is that none of the CMIP6 models simulate a TCR lower than their forced warming in 2020 (usually by a large margin; fig. S9). So, our finding of a forced 2020 warming of 1.2°C in the real world could contribute to discarding low TCR values—the use of improved GSAT observations plays a key role here.

Historical observations are expected to constrain ECS less effectively, and any such constraint must be taken with caution—estimating ECS from observations is equivalent to an extrapolation far outside the range of observed climate states. However, deriving implications

of our results for ECS remains of interest. Using CMIP6 models only, we find an ECS constrained range of 2.3 ° to 4.6°C, as compared to 2.1 ° to 6.1°C without the constraint. Consistent with other metrics, the model range is primarily revised downward, but our final constrained range excludes the lower end of the IPCC AR5–assessed likely range. We notice that our ECS range remains relatively wide, suggesting that observed GSAT changes do not constrain the long-term equilibrium (e.g., the ECS/TCR ratio) very well.

Comparing CMIP6 and CMIP5
Applying the same observational constraint using CMIP5 models and Representative Concentration Pathways (RCPs), instead of CMIP6 models and SSPs, is also of high interest (Fig. 4 and fig. S7). On average, the unconstrained CMIP6 ensemble projects a higher warming than CMIP5, consistent with a higher sensitivity (14). The CMIP6 ensemble also exhibits much wider uncertainty ranges, leading to a lower bound on 2100 projected warming lower than that of CMIP5. After applying the observational constraint, ranges agree remarkably well in the near term (e.g., before 2040), suggesting that observations play a dominant role in this time frame. CMIP5- and CMIP6-constrained ranges also exhibit comparable width for all scenarios and periods considered. However, they diverge somewhat in the late 21st century: The projected warming in 2100 is 10 to 15% higher using CMIP6,
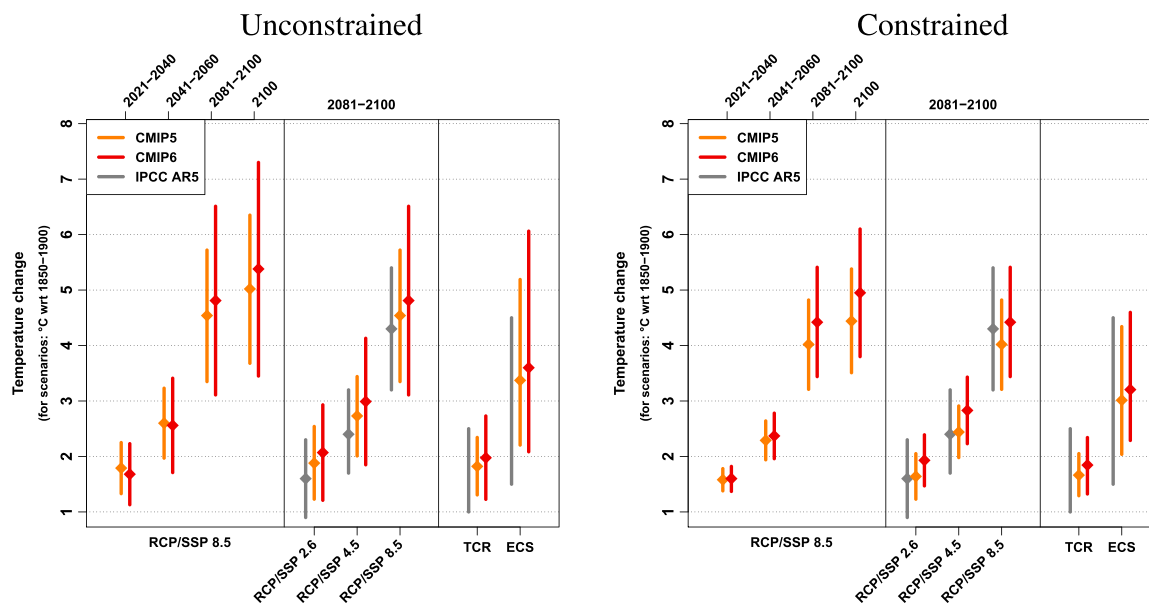
Fig. 4. Comparison of warming ranges from the CMIP6 ensemble to CMIP5 and IPCC AR5. Comparison of the unconstrained (**left**) and constrained (**right**) projected warming ranges in response to various emission scenarios and idealized experiments, as estimated using the CMIP5 [17 models, Representative Concentration Pathway (RCP) scenarios] and CMIP6 ensembles (22 models, SSP scenarios) to those assessed in the IPCC AR5 (*8*). Comparison is carried at different dates for a scenario (8.5 W m^{-2}; SSP5-8.5 in CMIP6, RCP8.5 in CMIP5, and IPCC AR5) over the 2081–2100 period for various emission scenarios and for the TCR and the ECS. Numbers for RCP scenarios in IPCC AR5 are taken from table 12.2 in (*8*) and shifted by +0.61°C (in agreement with the caption of that table) to account for the discrepancy in reference periods. TCR/ECS ranges from IPCC AR5 are assessed likely range (implying 66% confidence).

with the largest relative difference for the lowest emission scenarios. This corresponds to a 0.3° to 0.5°C difference in 2100, depending on the scenario. A smaller discrepancy is found in the case of climate sensitivity metrics, typically 5 to 10%. The range for TCR based on CMIP5 models is narrower, with a lower upper bound. The range for ECS is shifted upward by about 0.2°C from CMIP5 to CMIP6.

There are various explanations to these discrepancies. Differences in scenarios (*26*) contribute to a more pronounced 21st century warming in CMIP6 relative to CMIP5. Although RCPs and SSPs are scenarios with nominally the same forcing level in 2100, the actual forcing levels are higher in SSPs (including a higher GHG forcing; fig. S11) (*28*, *29*). Discrepancies in emission scenario contribute to the large gap found in the 21st century warming but cannot explain the reported difference in terms of TCR and ECS. The latter suggests that CMIP6 models might exhibit a higher sensitivity than CMIP5 models, not only in terms of the raw values (*14*) but also if taken conditionally to historical observations. In particular, we notice that the constrained time series of past changes using the CMIP5 or CMIP6 ensembles agree remarkably well. So, these two ensembles provide different estimates of future changes while they are in perfect agreement in the past. Two phenomena can explain or contribute to this. First, the historical forcings used in CMIP5 and CMIP6 differ substantially (fig. S11). The most notable difference is found in the late 20th century, involves the aerosols forcing, which is more negative in CMIP6, and exhibits a different time series. A more negative aerosol forcing can offset a larger fraction of GHG-induced warming, making the observational record consistent with higher sensitivity. Poor representation of radiative forcings after 2005 in CMIP5 simulations was also identified as contributing to a discrepancy between models and observations in terms of the recent warming trend (*30*). Second, progress in the representation of atmospheric

physics can affect how models respond to a given change in forcings. For instance, a higher ratio of ECS to TCR, nonlinearities in feedback or GHG forcing (*31*), could cause a different response to the same GHG emissions. Further research will be needed to quantify how these two terms (changes in radiative forcings versus changes internal to the models themselves) are contributing to the findings reported here. Last, the model sampling uncertainty (the number of models in both generations remains quite limited) could also contribute to the reported gap. This issue is further discussed below.

DISCUSSION

Because of an improved statistical method, we are able to make use of the entire observational record to refine estimates of past and future climate change. Our results suggest that historical observations can now be used to reduce uncertainty in human-induced warming significantly: typically by a factor of 3 in the past and in the near term (i.e., by 2040) and a factor of 2 in the long term (late 21st century). In this context, using an unconstrained multimodel ensemble is no longer the best choice for global mean temperature projections. This is an important finding because few observational constraints were applied to climate projections until recently (*8*). Overall, our results suggest that we are now at the time when direct monitoring of climate change enables narrowing uncertainty on both past and future warming substantially, as was expected (*4*, *32*).

We also derive constrained estimates of attributable warming to date, future warming in response to a range of emission scenarios, and metrics of climate sensitivity, all of them consistently rejecting the lower end of previous estimates. These results have broad implications in terms of foreseeable climate change impacts and the need for urgent mitigation.

A recent study (*15*) applied an observational constraint to CMIP6 projections using a different statistical approach. Our results agree with this study in rejecting the highest sensitivities from the CMIP6 ensemble. However, we report a larger reduction in uncertainty, arising primarily from discrepancies in the lower bound of constrained ranges. This is particularly clear in terms of constrained TCR ranges: 0.90° to 2.27°C in (*15*) (considering the 1981–2014 period), as opposed to 1.33 ° to 2.36°C here (both ranges are 5 to 95%). More work will be needed to fully understand this discrepancy, but we hypothesize that incorporating information about the total forced warming to date (i.e., considering a longer observed record) could contribute to rejecting low TCR values. Another noticeable discrepancy involves the CMIP5 versus CMIP6 comparison: Our observational constraint suggests a slightly higher future warming using the latest model generation, while Tokarska *et al.* (*15*) report consistent results with these two ensembles.

One potential limitation of this work is that our prior distribution might not sample uncertainty comprehensively. A first obvious limitation is related to the number of models (*22*), which remains modest. This number could increase as the CMIP6 archive becomes more fully populated. However, there are also important limitations related to the design of the CMIP exercises. CMIP ensembles are typically ensembles of opportunity, i.e., they are not designed to sample uncertainty comprehensively (*33*). For instance, no models are being intentionally built to provide low or high values of TCR or ECS, and the relatively wide ranges found among CMIP6 models was unintentional. Forcing uncertainty is also poorly sampled in the CMIP6 ensemble. The magnitude of the aerosol forcing in 2014 differs substantially among models (*29*), but uncertainty on the historical emissions of aerosols or aerosols precursors and their time series is not sampled. Last, CMIP models exhibit dependencies among themselves and from one generation to the next (*34*), further reducing the effective model sample size. To some extent, this model uncertainty sampling issue could be alleviated by some improvement of the statistical approach, e.g., using regularized estimates of the model error covariance. A better approach probably requires using perturbed physics ensembles (PPEs) (*35*), with an inclusion of forcing uncertainty, to overcome this limitation. However, production of such coordinated multimodel PPEs remains a challenge for the climate science community. In the meantime, CMIP ensembles remain the best available multimodel dataset to quantify uncertainties about future climate change.

The introduction of the new statistical method proposed in this study also opens new possibilities. Unlike techniques based on energy balance models, which are only suitable at the global or hemispheric scales (*11*), our technique could be easily adapted to constrain past and future changes at the regional scale. Incorporating spatial information, variables other than surface temperature, or other types of constraints (e.g., physically based or paleoclimate constraints), is another promising line of research. Given that accurate climate projections with well-quantified uncertainties are essential for adaptation planning and mitigation policies, we expect the results of this study and similar applications on smaller scales to be of great value to a range of stakeholders.

MATERIALS AND METHODS
Data
Observed data
We use observations from Cowtan and Way (*16*), hereafter denoted HadCRUT4-CW. This dataset provides an extension of the HadCRUT4

dataset (*36*) with global coverage, thus alleviating issues related to missing data. From this dataset, we compute the global mean near-surface temperature (GMST), without applying any observational mask. Furthermore, this dataset uses a blending of SSTs over ocean and near-surface air temperature over land. Several studies have shown that this metric of global mean temperature warms significantly less than the GSAT (*17*, *18*). To take this discrepancy into account, we multiply the Cowtan and Way GMST by a factor of 1.06, corresponding to a 6% increase (*16*). This factor was estimated in historical runs specifically, while previous calculations made over the 21st century range between 1.05 and 1.08 (*17*, *18*). In addition to affecting the long-term trend, this correction inflates the year-to-year variability in the observed time series.

The HadCRUT4-CW dataset is provided with an estimate of measurement uncertainties, through a set of equally plausible realizations (*36*). This is a remarkable feature, as HadCRUT4-CW is the only dataset with global coverage providing an estimate of observational uncertainty—which is why we chose to use this dataset. In the following, we take the median of this dataset as a best estimate. All realizations are used to estimate the measurement uncertainty. Note that we do not consider other datasets for GMST because they usually fall within the uncertainty of HadCRUT4-CW (*1*); considering the entire HadCRUT4-CW ensemble allows a more comprehensive treatment of uncertainty.

CMIP data
We make use of a large set of models from CMIP6 and CMIP5 (*13*, *37*). We took all models providing at least 200 years of preindustrial control simulations, one historical simulation, one 2.6 W m^{-2} of scenario (either RCP2.6 or SSP1-2.6), one 4.5 W m^{-2} of scenario, one 8.5 W m^{-2} of scenario, and either a histGHG simulation [i.e., a historical simulation in which GHGs follow their historical concentrations, while other forcings are kept constant (*38*)], or a 1% CO_2 simulation (in which the CO_2 concentration increases by 1% each year). Only the *tas* variable, corresponding to near-surface atmospheric temperature, is used here.

We consider 22 models from the CMIP6 ensemble: ACCESS-CM2, AWI-CM-1-1-MR, BCC-CSM2-MR, CAMS-CSM1-0, CanESM5, CESM2, CESM2-WACCM, CNRM-CM6-1, CNRM-CM6-1-HR, CNRM-ESM2-1, GFDL-ESM4, GISS-E2-1-G, HadGEM3-GC31-LL, INM-CM4-8, IPSL-CM6A-LR, MIROC-ES2L, MIROC6, MPI-ESM1-2-HR, MRI-ESM2-0, NESM3, NorESM2-LM, and UKESM1-0-LL. We consider 17 models from the CMIP5 ensemble: bcc-csm1-1, CanESM2, CCSM4, CESM1-CAM5, CNRM-CM5, CSIRO-Mk3-6-0, GFDL-CM3, GISS-E2-H, GISS-E2-R, HadGEM2-ES, IPSL-CM5A-LR, MIROC-ESM, MIROC-ESM-CHEM, MPI-ESM-LR, MPI-ESM-MR, MRI-CGCM3, and NorESM1-M.

TCRs and ECS of CMIP6 models were taken from (*15*) and recalculated following the same methodology for ACCESS-CM2 and AWI-CM-1-1-MR. TCR and ECS of CMIP5 models come from table 9.5 in (*39*).

Statistical method
Constraining projections
We first focus on the analysis of GSAT time series over the period 1850–2100, i.e., in response to historical forcings followed by a given emission scenario. We denote the real-world response to all forcings **x**. is a vector of size *n* = 251: the GSAT time series over the period 1850–2100 and under a given emission scenario. We denote the vector (time series) of GSAT observations **y**—these are available from 1850 to 2019 (i.e., **y** is of length n_y = 170).

The statistical approach works in two steps. First, we consider an ensemble of climate models to derive a (model-based) prior for **x**, denoted $\pi(\mathbf{x})$. Second, we make use of observations **y** to derive the posterior $p(\mathbf{x} \mid \mathbf{y})$.

To derive the prior $\pi(\mathbf{x})$, we start by estimating the forced GSAT response for each CMIP model (using all available members) and each scenario considered. This is performed using a generalized additive model (GAM), in which the response to NAT forcing is a rescaling of the response of an energy balance model, while the response to ANT forcings is only assumed to be smooth in time (smoothing splines are used to filter out part of internal variability). The procedure is identical to that described in (40); details are given in the Supplementary Materials. Then, we consider an ensemble of these forced responses (e.g., all CMIP6 or CMIP5 models) and derive the prior $\pi(\mathbf{x}) \sim N(\boldsymbol{\mu}, \boldsymbol{\Sigma}_{\text{mod}})$, assuming model-truth exchangeability (20, 41, 42), i.e., calculating $\boldsymbol{\mu}$ and $\boldsymbol{\Sigma}_{\text{mod}}$ as the sample mean and variance-covariance matrix over models. In this framework, $\boldsymbol{\Sigma}_{\text{mod}}$ quantifies the model uncertainty on the forced response **x**. This prior $\pi(\mathbf{x})$ can be interpreted as a first estimate of **x**, which makes no use of observations, and is based only on climate model simulations, with uncertainty based on model spread (8).

We further assume that observations **y** can be written as the sum of the forced response plus internal variability and measurement error, i.e.,

$$\mathbf{y} = \mathbf{H}\mathbf{x} + \boldsymbol{\varepsilon} \qquad (1)$$

where **H** is an observation operator and $\boldsymbol{\varepsilon}$ is a random term corresponding to measurement errors and internal variability. **H** basically extracts the part of **x** that is observed in **y**, i.e., the total forced response from 1850 to 2019. In the current application, **H** is a truncated $n_y \times n$ identity matrix, with 1 in the n_y diagonal coefficients and 0 elsewhere.

Under this assumption, the posterior distribution $p(\mathbf{x} \mid \mathbf{y})$ can be derived easily, as both $\pi(\mathbf{x})$ and $\boldsymbol{\varepsilon}$ follow normal laws. Details about this technical step are given in the Supplementary Materials.

Application to attribution

We now describe extension of our statistical method to the attribution problem. To estimate attributable warming, the method is applied to a much longer vector **x**: $\mathbf{x} = (\mathbf{x}^{\text{all}}; \mathbf{x}^{\text{nat}}; \mathbf{x}^{\text{ghg}})$, where $\mathbf{x}^{\text{all}}$, $\mathbf{x}^{\text{nat}}$, and $\mathbf{x}^{\text{ghg}}$ describe the responses to ALL, NAT-only, or GHG-only forcings, respectively. $\mathbf{x}^{\text{all}}$ and $\mathbf{x}^{\text{nat}}$ both cover the period 1850–2100, but $\mathbf{x}^{\text{ghg}}$ is restricted to the period 1850–2020 [as we only consider histGHG simulations (38)]. Therefore, **x** has a total dimension of $n_a = 251 + 251 + 171 = 673$ in this case. **H** has to be adapted accordingly and becomes a $n_y \times n_a$ matrix

$$\mathbf{H} = [\mathbf{I}_{n_y} \, 0 \, 0] \qquad (2)$$

where each block corresponds to one ALL, NAT, or GHG component and where $\mathbf{I}_{n_y}$ is a truncated identity matrix of size $n_y \times n$. As observations have been made in the presence of all forcings, **H** simply extracts values of $\mathbf{x}^{\text{all}}$ at observed dates—and the other components of **x** are not "observed." The remaining of the method is unchanged. The posterior distribution $p(\mathbf{x} \mid \mathbf{y})$ then provides information not only about the total forced response given **y** but also about the responses to NAT and GHG forcings specifically, still given **y**. Estimates of the responses to other combinations of forcings such as ANT or OA can be derived by subtraction. For instance, the prior

and posterior distributions of $\mathbf{x}^{\text{ant}} := \mathbf{x}^{\text{all}} - \mathbf{x}^{\text{nat}}$ can be easily deduced from those of the full vector $\mathbf{x} = (\mathbf{x}^{\text{all}}; \mathbf{x}^{\text{nat}}; \mathbf{x}^{\text{ghg}})$. The proposed technique is very similar, although not strictly identical, to that introduced in (20) (further discussion in the Supplementary Materials).

Deriving the prior $\pi(\mathbf{x})$, in the case of attribution, requires an estimate of the responses of each climate model considered to the NAT and GHG forcings, specifically. The NAT component is taken from the GAM decomposition mentioned above. Estimation of the GHG component requires a specific analysis. For some CMIP6 models, histGHG simulations are available and cover the full 1850–2020 period; in this case, $\mathbf{x}^{\text{ghg}}$ is estimated from these simulations, using a basic smoothing procedure. For other models, the histGHG simulation do not cover the entire 1850–2020 period, and we use an adaptation of our Kriging technique to produce a statistical completion of that simulation over 1850–2020. Last, some models did not perform any histGHG simulation, and then we use another adaptation of our Kriging technique to reconstruct them statistically, using 1% CO_2 and an extended historical run as inputs. Details regarding estimation of $\mathbf{x}^{\text{ghg}}$ are given in the Supplementary Materials. Ignoring reconstructed $\mathbf{x}^{\text{ghg}}$ responses in the attribution analysis leads to slightly narrower confidence ranges (fig. S8). This suggests that the main analysis shown in Fig. 1 is conservative.

Application to TCR and ECS

Another extension of our statistical technique concerns metrics of climate sensitivity, i.e., TCR and ECS. A key difficulty, in this case, is that there are several ways to relate TCR and ECS to the constrained temperature changes. The method used to produce Fig. 2 involves applying the observational constraint to a vector

$$\mathbf{x} = (\mathbf{x}^{\text{all}}, \text{TCR}, F, \log(-\lambda)) \qquad (3)$$

where F is the radiative forcing corresponding to a doubling of CO_2 concentration, λ is the feedback parameter, and $\text{ECS} = -\frac{F}{\lambda}$ (43). Calculating ECS that way means that the feedback parameter λ is assumed constant; therefore, we consider an effective climate sensitivity rather than the real long-term ECS (44). As for other applications, this vector **x** is assumed to follow a Gaussian prior. This formulation ensures that λ is negative (a desirable property). However, there are other valid options to relate ECS to changes in $\mathbf{x}^{\text{all}}$ (see discussion in the Supplementary Materials). Among the three options tested, constrained ranges for ECS agree reasonably well (fig. S10).

Discussion of the method and estimation of input parameters

Applying the observational constraint this way offers many advantages. The model prior captures various facets of model uncertainty in a consistent way. This includes uncertainty in both the magnitude and the temporal pattern of the forced response, unlike usual D&A methods (6, 7, 10, 19, 20, 27). Using the entire observed dataset avoids the arbitrary choice of a reference period (as performed, e.g., for historical trends), facilitates annual updates, and helps distinguish the responses to GHGs from OA factors (thanks to the different emission time series for these two forcings). In addition, the entire time series of constrained projections is derived in a consistent way, which is particularly attractive for near-term projections.

Our procedure can be considered as an adaptation of Kriging or Gaussian process regression (45, 46)—a method developed to interpolate geophysical data based on prior covariances. Here, this technique is used to extrapolate past changes into the future, using climate models as a learning sample. One noticeable difference with a standard use of Kriging resides in the prior, which, in our case, is nonstationary

and derived from physically based climate models. In this statistical procedure, one could also identify all components of a Kalman filtering procedure, as used in data assimilation and weather forecasting systems: a model or background error covariance Σ_{mod}, observation error covariance Σ_{obs}, and the observation operator H. However, unlike in data assimilation, there is no iteration—our procedure could be considered as a one-step filtering.

Overall, application of this technique requires to specify what x and y are and how the key components μ, Σ_{mod}, and Σ_{obs} are estimated. In practice, μ and Σ_{mod} are derived as the sample mean and variance-covariance matrix of an ensemble of climate model responses. Given the limited number of available models, Σ_{mod} is highly degenerate. Σ_{obs} is a covariance matrix describing observational uncertainty. We assume that $\Sigma_{obs} = \Sigma_{meas.} + \Sigma_{i.\,v.}$, where $\Sigma_{meas.}$ is the measurement error, while $\Sigma_{i.\,v.}$ describes internal variability. $\Sigma_{meas.}$ is simply estimated as the sample variance-covariance matrix of the HadCRUT4-CW ensemble. Estimation of $\Sigma_{i.\,v.}$ is based on a mixture of two autoregressive processes of order 1 (AR1), with different time scales. We assume that internal variability ε_t writes

$$\varepsilon_t \sim \sigma_{fast}^2 AR1(\alpha_{fast}) + \sigma_{slow}^2 AR1(\alpha_{slow}) \qquad (4)$$

with $\alpha_{slow} > \alpha_{fast}$. To estimate the coefficients ($\sigma_{fast}^2, \alpha_{fast}, \sigma_{slow}^2$, and α_{slow}), we compute observational residuals (i.e., we subtract the CMIP6 multimodel mean time series to observations, y) and then apply a maximum likelihood procedure to these residuals. Uncertainty on these estimated coefficients is not taken into account. Our estimate of $\Sigma_{i.v.}$ is consistent with previous studies reporting that GSAT internal variability exhibits more dependence than AR1 but less than a long-range memory effect (47, 48). Further discussion and justification for this choice are provided in the Supplementary Materials.

SUPPLEMENTARY MATERIALS

REFERENCES AND NOTES
1. IPCC, An IPCC special report on the impacts of global warming of 1.5°C above pre-industrial levels and related global greenhouse gas emission pathways, in the context of strengthening the global response to the threat of climate change, sustainable development, and efforts to eradicate poverty, in *Global Warming of 1.5°C*, V. Masson-Delmotte, P. Zhai, H. O. Pörtner, D. Roberts, J. Skea, P. R. Shukla, A. Pirani, W. Moufouma-Okia, C. Péan, R. Pidcock, S. Connors, J. B. R. Matthews, Y. Chen, X. Zhou, M. I. Gomis, E. Lonnoy, T. Maycock, M. Tignor, T. Waterfield, Eds. (IPCC, 2018).
2. C. E. Forest, M. R. Allen, P. H. Stone, A. P. Sokolov, Constraining uncertainties in climate models using climate change detection techniques. *Geophys. Res. Lett.* **27**, 569–572 (2000).
3. M. R. Allen, P. A. Stott, J. F. B. Mitchell, R. Schnur, T. L. Delworth, Quantifying the uncertainty in forecasts of anthropogenic climate change. *Nature* **407**, 617–620 (2000).
4. P. A. Stott, J. A. Kettleborough, Origins and estimates of uncertainty in predictions of twenty-first century temperature rise. *Nature* **416**, 723–726 (2002).
5. J. A. Kettleborough, B. B. B. Booth, P. A. Stott, M. R. Allen, Estimates of uncertainty in predictions of global mean surface temperature. *J. Climate* **20**, 843–855 (2007).
6. P. Stott, P. Good, A. Jones, N. Gillett, E. Hawkins, The upper end of climate model temperature projections is inconsistent with past warming. *Environ. Res. Lett.* **8**, 014024 (2013).
7. N. P. Gillett, V. K. Arora, D. Matthews, M. R. Allen, Constraining the ratio of global warming to cumulative CO₂ emissions using CMIP5 simulations. *J. Climate* **26**, 6844–6858 (2013).
8. M. Collins, R. Knutti, J. Arblaster, J.-L. Dufresne, T. Fichefet, P. Friedlingstein, X. Gao, W. J. Gutowski, T. Johns, G. Krinner, M. Shongwe, C. Tebaldi, A. J. Weaver, M. Wehner, in *Climate change 2013: The Physical Science Basis. Contribution of Working Group I to the Fifth Assessment Report of the Intergovernmental Panel on Climate Change* (Cambridge Univ. Press, 2013), pp. 1029–1136.
9. R. Knutti, M. A. A. Rugenstein, G. C. Hegerl, Beyond equilibrium climate sensitivity. *Nat. Geosci.* **10**, 727–736 (2017).
10. A. Schurer, G. Hegerl, A. Ribes, D. Polson, C. Morice, S. Tett, Estimating the transient climate response from observed warming. *J. Climate* **31**, 8645–8663 (2018).
11. K. Haustein, F. E. L. Otto, V. Venema, P. Jacobs, K. Cowtan, Z. Hausfather, R. G. Way, B. White, A. Subramanian, A. P. Schurer, A limited role for unforced internal variability in twentieth-century warming. *J. Climate* **32**, 4893–4917 (2019).
12. A. Otto, F. E. L. Otto, O. Boucher, J. Church, G. Hegerl, P. M. Forster, N. P. Gillett, J. Gregory, G. C. Johnson, R. Knutti, N. Lewis, U. Lohmann, J. Marotzke, G. Myhre, D. Shindell, B. Stevens, M. R. Allen, Energy budget constraints on climate response. *Nat. Geosci.* **6**, 415–416 (2013).
13. V. Eyring, S. Bony, G. A. Meehl, C. A. Senior, B. Stevens, R. J. Stouffer, K. E. Taylor, Overview of the coupled model intercomparison project phase 6 (CMIP6) experimental design and organization. *Geosci. Model Dev.* **9**, 1937–1958 (2016).
14. P. M. Forster, A. C. Maycock, C. M. McKenna, C. J. Smith, Latest climate models confirm need for urgent mitigation. *Nat. Clim. Change* **10**, 7–10 (2019).
15. K. B. Tokarska, M. B. Stolpe, S. Sippel, E. M. Fischer, C. J. Smith, F. Lehner, R. Knutti, Past warming trend constrains future warming in CMIP6 models. *Sci. Adv.* **6**, eaaz9549 (2020).
16. K. Cowtan, R. G. Way, Coverage bias in the hadcrut4 temperature series and its impact on recent temperature trends. *Q. J. Roy. Meteorol. Soc.* **140**, 1935–1944 (2014).
17. K. Cowtan, Z. Hausfather, E. Hawkins, P. Jacobs, M. E. Mann, S. K. Miller, B. A. Steinman, M. B. Stolpe, R. G. Way, Robust comparison of climate models with observations using blended land air and ocean sea surface temperatures. *Geophys. Res. Lett.* **42**, 6526–6534 (2015).
18. M. Richardson, K. Cowtan, R. J. Millar, Global temperature definition affects achievement of long-term climate goals. *Environ. Res. Lett.* **13**, 054004 (2018).
19. G. S. Jones, P. A. Stott, J. F. B. Mitchell, Uncertainties in the attribution of greenhouse gas warming and implications for climate prediction. *J. Geophys. Res. Atmos.* **121**, 6969–6992 (2016).
20. A. Ribes, F. W. Zwiers, J.-M. Azaïs, P. Naveau, A new statistical approach to climate change detection and attribution. *Climate Dynam.* **48**, 367–386 (2017).
21. A. G. Libardoni, C. E. Forest, A. P. Sokolov, E. Monier, Underestimating internal variability leads to narrow estimates of climate system properties. *Geophys. Res. Lett.* **46**, 10000–10007 (2019).
22. P. Goodwin, A. Katavouta, V. M. Roussenov, G. L. Foster, E. J. Rohling, R. G. Williams, Pathways to 1.5°C and 2°C warming based on observational and geological constraints. *Nat. Geosci.* **11**, 102–107 (2018).
23. N. Bindoff, P. Stott, K. AchutaRao, M. Allen, N. Gillett, D. D. Gutzler, K. K. Hansingo, G. Hegerl, Y. Hu, S. Jain, I. Mokhov, J. Overland, J. Perlwitz, R. Sebbari, X. Zhang, Detection and attribution of climate change: From global to regional, in *Climate Change 2013: The Physical Science Basis. Contribution of Working Group I to the Fifth Assessment Report of the Intergovernmental Panel on Climate Change*, T. F. Stocker, D. Qin, G.-K. Plattner, M. Tignor, S. K. Allen, J. Boschung, A. Nauels, Y. Xia, V. Bex, P. M. Midgley, Eds. (Cambridge Univ. Press, 2013), pp. 867–952.
24. A. P. Schurer, M. E. Mann, E. Hawkins, S. F. Tett, G. C. Hegerl, Importance of the pre-industrial baseline for likelihood of exceeding Paris goals. *Nat. Clim. Change* **7**, 563–567 (2017).
25. K. Haustein, M. Allen, P. Forster, F. Otto, D. Mitchell, H. Matthews, D. Frame, A real-time global warming index. *Sci. Rep.* **7**, 15417 (2017).
26. B. C. O'Neill, C. Tebaldi, D. P. van Vuuren, V. Eyring, P. Friedlingstein, G. Hurtt, R. Knutti, E. Kriegler, J.-F. Lamarque, J. Lowe, G. A. Meehl, R. Moss, K. Riahi, B. M. Sanderson, The scenario model intercomparison project (ScenarioMIP) for CMIP6. *Geosci. Model Dev.* **9**, 3461–3482 (2016).
27. A. Ribes, L. Terray, Application of regularised optimal fingerprinting to attribution. Part ii: Application to global near-surface temperature. *Climate Dynam.* **41**, 2837–2853 (2013).
28. Z. R. J. Nicholls, M. Meinshausen, J. Lewis, R. Gieseke, D. Dommenget, K. Dorheim, C.-S. Fan, J. S. Fuglestvedt, T. Gasser, U. Golüke, P. Goodwin, E. Kriegler, N. J. Leach, D. Marchegiani, Y. Quilcaille, B. H. Samset, M. Sandstad, A. N. Shiklomanov, R. B. Skeie, C. J. Smith, K. Tanaka, J. Tsutsui, Z. Xie, Reduced complexity model intercomparison project phase 1: Protocol, results and initial observations. *Geosci. Model Dev.* **2020**, 1–33 (2020).
29. C. J. Smith, R. J. Kramer, G. Myhre, K. Alterskjær, W. Collins, A. Sima, O. Boucher, J.-L. Dufresne, P. Nabat, M. Michou, S. Yukimoto, J. Cole, D. Paynter, H. Shiogama, F. M. O'Connor, E. Robertson, A. Wiltshire, T. Andrews, C. Hannay, R. Miller, L. Nazarenko, A. Kirkevåg, D. Olivié, S. Fiedler, A. Lewinschal, C. Mackallah, M. Dix, R. Pincus, P. M. Forster, Effective radiative forcing and adjustments in CMIP6 models. *Atmospheric Chem. Phys.* **20**, 9591–9618 (2020).
30. G. A. Schmidt, D. T. Shindell, K. Tsigaridis, Reconciling warming trends. *Nat. Geosci.* **7**, 158–160 (2014).
31. O. Geoffroy, D. Saint-Martin, Equilibrium-and transient-state dependencies of climate sensitivity: Are they important for climate projections? *J. Climate* **33**, 1863–1879 (2019).

32. G. Myhre, O. Boucher, F.-M. Bréon, P. Forster, D. Shindell, Declining uncertainty in transient climate response as CO_2 forcing dominates future climate change. *Nat. Geosci.* **8**, 181–185 (2015).

33. R. Knutti, R. Furrer, C. Tebaldi, J. Cermak, G. A. Meehl, Challenges in combining projections from multiple climate models. *J. Climate* **23**, 2739–2758 (2010).

34. R. Knutti, D. Masson, A. Gettelman, Climate model genealogy: Generation cmip5 and how we got there. *Geophys. Res. Lett.* **40**, 1194–1199 (2013).

35. J. M. Murphy, B. B. B. Booth, M. Collins, G. R. Harris, D. M. Sexton, M. J. Webb, A methodology for probabilistic predictions of regional climate change from perturbed physics ensembles. *Philos. Trans. R. Soc. A* **365**, 1993–2028 (2007).

36. C. P. Morice, J. J. Kennedy, N. A. Rayner, P. D. Jones, Quantifying uncertainties in global and regional temperature change using an ensemble of observational estimates: The hadCRUT4 data set. *J. Geophys. Res.* **117**, D08101 (2012).

37. K. E. Taylor, R. J. Stouffer, G. A. Meehl, An overview of CMIP5 and the experiment design. *Bull. Am. Meteorol. Soc.* **93**, 485–498 (2012).

38. N. P. Gillett, H. Shiogama, B. Funke, G. Hegerl, R. Knutti, K. Matthes, B. D. Santer, D. Stone, C. Tebaldi, The detection and attribution model intercomparison project (DAMIP v1.0) contribution to CMIP6. *Geosci. Model Dev.* **9**, 3685–3697 (2016).

39. G. Flato, J. Marotzke, B. Abiodun, P. Braconnot, S. C. Chou, W. Collins, P. Cox, F. Driouech, S. Emori, V. Eyring, C. Forest, P. Gleckler, E. Guilyardi, C. Jakob, V. Kattsov, C. Reason, M. Rummukainen, in *Climate change 2013: The Physical Science Basis. Contribution of Working Group I to the Fifth Assessment Report of the Intergovernmental Panel on Climate Change* (Cambridge Univ. Press, 2014), pp. 741–866.

40. A. Ribes, S. Thao, J. Cattiaux, Describing the relationship between a weather event and climate change: A new statistical approach. *J. Climate* **33**, 6297–6314 (2020).

41. J. D. Annan, J. C. Hargreaves, Reliability of the CMIP3 ensemble. *Geophys. Res. Lett.* **37**, L02703 (2010).

42. J. Rougier, M. Goldstein, L. House, Second-order exchangeability analysis for multimodel ensembles. *J. Am. Stat. Assoc.* **108**, 852–863 (2013).

43. J. M. Gregory, W. J. Ingram, M. A. Palmer, G. S. Jones, P. A. Stott, R. B. Thorpe, J. A. Lowe, T. C. Johns, K. D. Williams, A new method for diagnosing radiative forcing and climate sensitivity. *Geophys. Res. Lett.* **31**, L03205 (2004).

44. S. C. Sherwood, M. J. Webb, J. D. Annan, K. C. Armour, P. M. Forster, J. C. Hargreaves, G. Hegerl, S. A. Klein, K. D. Marvel, E. J. Rohling, M. Watanabe, T. Andrews, P. Braconnot, C. S. Bretherton, G. L. Foster, Z. Hausfather, A. S. von der Heydt, R. Knutti, T. Mauritsen, J. R. Norris, C. Proistosescu, M. Rugenstein, G. A. Schmidt, K. B. Tokarska, M. D. Zelinka, An assessment of Earth's climate sensitivity using multiple lines of evidence. *Rev. Geophys.* **58**, e2019RG000678 (2020).

45. N. Cressie, *Statistics for Spatial Data* (Wiley Online Library, 1992).

46. C. K. Williams, C. E. Rasmussen, *Gaussian Processes for Machine Learning* (MIT Press, 2006), vol. 2.

47. J. Imbers, A. Lopez, C. Huntingford, M. Allen, Sensitivity of climate change detection and attribution to the characterization of internal climate variability. *J. Climate* **27**, 3477–3491 (2014).

48. D. I. Vyushin, P. J. Kushner, F. Zwiers, Modeling and understanding persistence of climate variability. *J. Geophys. Res.* **117**, D21106 (2012).

49. C. J. Smith, R. J. Kramer, G. Myhre, P. M. Forster, B. J. Soden, T. Andrews, O. Boucher, G. Faluvegi, D. Fläschner, Ø. Hodnebrog, M. Kasoar, V. Kharin, A. Kirkevåg, J.-F. Lamarque, J. Mülmenstädt, D. Olivié, T. Richardson, B. H. Samset, D. Shindell, P. Stier, T. Takemura, A. Voulgarakis, D. Watson-Parris, Understanding rapid adjustments to diverse forcing agents. *Geophys. Res. Lett.* **45**, 12,023–12,031 (2018).

50. M. E. Mann, S. Rahmstorf, B. A. Steinman, M. Tingley, S. K. Miller, The likelihood of recent record warmth. *Sci. Rep.* **6**, 19831 (2016).

51. O. Geoffroy, D. Saint-Martin, D. J. L. Olivié, A. Voldoire, G. Bellon, S. Tytéca, Transient climate response in a two-layer energy-balance model. part I: Analytical solution and parameter calibration using CMIP5 aogcm experiments. *J. Climate* **26**, 1841–1857 (2013).

52. T. Gneiting, A. E. Raftery, A. H. Westveld III, T. Goldman, Calibrated probabilistic forecasting using ensemble model output statistics and minimum CRPS estimation. *Mon. Weather Rev.* **133**, 1098–1118 (2005).

Citation: A. Ribes, S. Qasmi, N. P. Gillett, Making climate projections conditional on historical observations. *Sci. Adv.* **7**, eabc0671 (2021).

Science Advances

Making climate projections conditional on historical observations

Aurélien Ribes, Saïd Qasmi and Nathan P. Gillett

ARTICLE TOOLS	http://advances.sciencemag.org/content/7/4/eabc0671
SUPPLEMENTARY MATERIALS	http://advances.sciencemag.org/content/suppl/2021/01/14/7.4.eabc0671.DC1
REFERENCES	This article cites 46 articles, 1 of which you can access for free http://advances.sciencemag.org/content/7/4/eabc0671#BIBL
PERMISSIONS	http://www.sciencemag.org/help/reprints-and-permissions